HHS Public Access

Author manuscript

J Mech Behav Biomed Mater. Author manuscript; available in PMC 2020 August 01.

Published in final edited form as:

J Mech Behav Biomed Mater. 2019 August ; 96: 165–171. doi:10.1016/j.jmbbm.2019.04.014.

Bioengineered analog of stromal cell-derived factor 1α preserves the biaxial mechanical properties of native myocardium after infarction

Hanjay Wang[a], **Andrew Wisneski**[b], **Michael J. Paulsen**[a], **Annabel Imbrie-Moore**[a,c], **Zhongjie Wang**[b], **Yue Xuan**[b], **Hector Lopez Hernandez**[d], **Haley J. Lucian**[a], **Anahita Eskandari**[a], **Akshara D. Thakore**[a], **Justin M. Farry**[a], **Camille E. Hironaka**[a], **Daniel von Bornstaedt**[a], **Amanda N. Steele**[a,e], **Lyndsay M. Stapleton**[a,e], **Kiah M. Williams**[a], **Matthew A. Wu**[a], **John W. MacArthur Jr.**[a], **Y. Joseph Woo**[a,e,*]

[a]Department of Cardiothoracic Surgery, Stanford University, Stanford, CA, USA

[b]Department of Surgery, University of California San Francisco, San Francisco, CA, USA

[c]Department of Mechanical Engineering, Stanford University, Stanford, CA, USA

[d]Department of Materials Science and Engineering, Stanford University, Stanford, CA, USA

[e]Department of Bioengineering, Stanford University, Stanford, CA, USA

Abstract

Adverse remodeling of the left ventricle (LV) after myocardial infarction (MI) results in abnormal tissue biomechanics and impaired cardiac function, often leading to heart failure. We hypothesized that intramyocardial delivery of engineered stromal cell-derived factor 1α analog (ESA), our previously-developed supra-efficient proangiogenic chemokine, preserves biaxial LV mechanical properties after MI. Male Wistar rats (n = 45) underwent sham surgery (n = 15) or permanent left anterior descending coronary artery ligation. Rats sustaining MI were randomized for intramyocardial injections of either saline (100 μL, n = 15) or ESA (6 μg/kg, n = 15), delivered at four standardized borderzone sites. After 4 weeks, echocardiography was performed, and the hearts were explanted. Tensile testing of the anterolateral LV wall was performed using a displacement-controlled biaxial load frame, and modulus was determined after constitutive modeling. At 4 weeks post-MI, compared to saline controls, ESA-treated hearts had greater wall thickness (1.68 ± 0.05 mm vs 1.42 ± 0.08 mm, p = 0.008), smaller end-diastolic LV internal dimension (6.88 ± 0.29 mm vs 7.69 ± 0.22 mm, p = 0.044), and improved ejection fraction (62.8 ± 3.0% vs 49.4 ± 4.5%, p = 0.014). Histologic analysis revealed significantly reduced infarct size for ESA-treated hearts compared to saline controls (29.4 ± 2.9% vs 41.6 ± 3.1%, p = 0.021). Infarcted hearts treated with ESA exhibited decreased modulus compared to those treated with saline in both the circumferential (211.5 ± 6.9 kPa vs 264.3 ± 12.5 kPa, p = 0.001) and longitudinal axes (194.5 ± 6.5 kPa vs 258.1 ± 14.4 kPa, p < 0.001). In both principal directions,

*Corresponding author. Department of Cardiothoracic Surgery, Stanford University, Falk Building CV-235, 300 Pasteur Drive, Stanford, CA, 94305-5407, USA. joswoo@stanford.edu (Y.J. Woo).

Declarations of interest

None.

ESA-treated infarcted hearts possessed similar tissue compliance as sham non-infarcted hearts. Overall, intramyocardial ESA therapy improves post-MI ventricular remodeling and function, reduces infarct size, and preserves native LV biaxial mechanical properties.

Keywords

Biaxial tension; Myocardial infarction; Ventricular remodeling; Angiogenic therapy

1. Introduction

After myocardial infarction (MI), adverse pathological remodeling ensues, resulting in altered pump mechanics and ventricular dysfunction (Holmes et al., 2005). While the initial response to cardiomyocyte necrosis involves cellular inflammation and edema, a prolonged phase of fibroblast proliferation and collagen deposition results in progressive scar formation, tissue stiffening, and left ventricular (LV) thinning with dilation during the subsequent weeks of infarct healing (Gupta et al., 1994; Lerman et al., 1983; Pfeffer et al., 1979). LV dilatation compensates for impaired function by normalizing stroke volume, but also increases wall stress based on Laplace's Law, thereby stimulating further chamber enlargement affecting both the infarcted and adjacent non-infarcted myocardium (Pfeffer and Braunwald, 1990). Expansion of this perfused but hypocontractile borderzone contributes to the vicious cycle that ultimately results in decompensated heart failure (Jackson et al., 2002; Narula et al., 2000).

Therapies that minimize the degree of borderzone expansion and modulate the mechanical properties of infarcted myocardium have significant potential to improve both survival and quality of life for patients with ischemic heart disease (Clarke et al., 2016). Stromal cell-derived factor 1α (SDF), a chemokine that attracts bone marrow-derived endothelial progenitor stem cells (EPCs), has been shown to increase microvascular density, maintain cardiomyocyte survival, reduce infarct size, inhibit borderzone expansion, attenuate adverse remodeling, and preserve LV function after MI (Atluri et al., 2013, 2006; Woo et al., 2005; Ziff et al., 2018). Using computational protein modeling, we previously designed an engineered SDF analog (ESA) and demonstrated its supra-efficient activity in both small and large animal MI models (Hiesinger et al., 2012, 2011; Macarthur et al., 2014).

Uniaxial tensile testing of longitudinal strips of infarcted myocardium treated with ESA previously suggested preservation of both tensile modulus and viscoelastic properties in association with improved LV function after MI (MacArthur et al., 2013; Trubelja et al., 2014). However, due to the intrinsic anisotropy of myocardial tissues (Demer and Yin, 1983; Gupta et al., 1994; Omens et al., 1993), as well as the variation of myocyte fiber orientation and mechanical properties at different depths within the LV wall (Harrington et al., 2005; Novak et al., 1994), uniaxial data alone is insufficient for a full mechanical characterization of the tissue (Demer and Yin, 1983). A multiaxial analysis including both the longitudinal and circumferential axes is therefore necessary to obtain a more thorough biomechanical evaluation of the efficacy of ESA.

In this study, we perform planar biaxial tensile testing of passive rat LV myocardium, comparing the mechanical properties of infarcted hearts with and without intramyocardial ESA therapy. We hypothesized that local delivery of ESA to the borderzone at the time of MI preserves biaxial LV mechanical properties after 4 weeks.

2. Materials and methods

2.1. Protein design and synthesis

Our design of ESA was previously described in detail (Hiesinger et al., 2011). Briefly, the central β-pleated sheet of SDF was replaced with a diproline linker, thus preserving the natural three-dimensional orientation of the retained N-terminal CXCR4 receptor-binding domain and the C-terminal stabilization domain of SDF. ESA was synthesized using solid-phase peptide synthesis (AnaSpec, Fremont, CA).

2.2. Animal care and biosafety

Male Wistar rats (270–330 g) were obtained from Charles River Laboratories (Wilmington, MA). Food and water were provided ad libitum. All experiments involving animals were performed in accordance with the Guide for the Care and Use of Laboratory Animals published by the United States National Institutes of Health (8th Edition, 2011). The experimental protocol was approved by the Institutional Animal Care and Use Committee at Stanford University (Protocol 28921).

2.3. Ischemic cardiomyopathy model

Rats (n = 30) underwent surgical induction of MI by ligation of the left anterior descending (LAD) coronary artery. The animals were anesthetized with 2% isoflurane (Fluriso™, VetOne) at a flow rate of 2 L/min. Endotracheal intubation was achieved with a 16 G angiocatheter, and the animals were mechanically ventilated (Hallowell EMC, Pittsfield, MA) with continuous 1–2% isoflurane for maintenance of anesthesia. A thoracotomy was performed through the left fourth intercostal space to expose the heart, and the LAD was directly visualized. A 6–0 polypropylene suture was placed around the LAD approximately 1 mm below the left atrial appendage. The suture was snared, and the area of resulting LV pallor was assessed to ensure consistently-sized infarcts. The suture was then permanently tied to produce a large anterolateral MI. The animals were randomized to receive either phosphate-buffered saline (PBS, 100 μL, n = 15) or ESA (6 μg/kg in 100 μL, n = 15), injected intramyocardially at 4 standardized border-zone sites immediately following LAD occlusion (Fig. 1A). An additional group of animals underwent sham surgery (n = 15), in which the pericardium was opened and the heart exposed, but myocardial ischemia was not induced. Finally, the thoracotomy was closed in layers, and the animals were extubated and recovered.

2.4. Echocardiography

Echocardiography was performed 4 weeks after MI or sham surgery for all animals. Left parasternal LV short and long axis views, including B- and M-mode images, were acquired using a Vevo Imaging Station (VisualSonics Inc., Toronto, Canada) equipped with a Vevo 2100 system and an ultra-high frequency linear array transducer (MicroScan™ MS250 13–

24 MHz transducer, VisualSonics Inc.). Image analysis was performed using Vevo LAB software (VisualSonics Inc.), including measurements of LV wall thickness in diastole over the anterolateral LAD territory (LVWT), LV internal diameter in systole (LVIDs) and diastole (LVIDd), and ejection fraction (EF) at the level of the mid-papillary muscles (Brown et al., 2002). Echocardiographic image acquisition and analysis were performed by a single individual to reduce interobserver bias.

2.5. Heart explant and sample preparation

Following echocardiography 4 weeks after the initial surgery, the rats were anesthetized and underwent median sternotomy. University of Wisconsin (UW®) cold cardioplegic storage solution (Bridge to Life Ltd., Columbia, SC) was delivered by intracardiac injection via the right ventricle to induce diastolic arrest. The heart was explanted and placed in a dish of 4°C PBS for dissection. The right ventricle was excised, and incisions were made along the anterior and posterior LV-septal junctions to remove the septal tissue (Fig. 1B). The LV wall was unrolled circumferentially, and the lateral-most aspect of the LV (representing non-LAD territory) was removed to produce an approximately 10 mm × 10 mm square of anterolateral LV wall tissue (Fig. 1C). The samples were stored in UW solution at 4°C until use to avoid contracture.

2.6. Planar biaxial tensile testing

Planar biaxial tensile testing was performed using a custom-built, displacement-controlled biaxial load frame (Azadani et al., 2012; Mookhoek et al., 2017). Two 5–0 polypropylene sutures were anchored to each edge of the myocardial sample using hooks and then fixed to the four arms of the biaxial stretcher, mounting the circumferential and longitudinal axes of the myocardium along the principal axes of deformation (Fig. 1D). Five 250–355 μm black ceramic marker beads (MO-SCI Corporation, Rolla, MO) were placed on the tissue surface in a 4 mm square in the center of the sample. Fixative agents, which may introduce potential confounding mechanical effects, were unnecessary, as the beads consistently remained in place while the samples were floated in PBS at room temperature during subsequent mechanical testing. The load cells (model 31/3672–02, 1000 g; Honeywell Sensotec, Columbus, OH) on two orthogonal arms of the stretcher were zeroed with the sample fully relaxed. Load cell data was used to determine the forces imparted on the sample during deformation. Images of the tissue surface during deformation were recorded in real time using a charge-coupled device camera (model TM 9701; 300 frames/sec, 0.1 pixels/mm; Pulnix, Sunnyvale, CA) positioned directly above the sample. Strains in the principal directions were calculated based on relative marker bead movements, tracked using LabVIEW (National Instruments, Austin, TX). All samples were tested using the same biaxial displacement-controlled protocol. First, all samples were pre-loaded to 0.05 N in both axes, and 20 preconditioning cycles of 4% strain were performed at 1% strain/sec (MacArthur et al., 2013). Immediately afterward, each sample underwent three consecutive cycles up to 40% peak strain, conservatively encompassing the full range of physiologic strains observed in rat hearts (Weytjens et al., 2008). Stress-strain data from the final stretching cycle was used for analysis. All samples were tested within 6 h of heart explant. Accuracy of the biaxial load cells and stretching apparatus was ensured by retesting samples after 90° rotation, which produced no discrepancies.

2.7. Constitutive modeling and data analysis

Experimental Cauchy stress (T^{exp}) in the circumferential (θ) and longitudinal (L) myocardial directions was calculated by the equations below, where F is the force measured by the load cells during deformation, t is tissue thickness measured by echocardiography, and λ is the ratio of deformed length to resting tissue length (l).

$$T_{\theta\theta}^{exp} = \lambda_\theta \frac{F_\theta}{t l_L} \quad (1a)$$

$$T_{LL}^{exp} = \lambda_L \frac{F_L}{t l_\theta} \quad (1b)$$

Green strain (E) was calculated in each direction using the equations below:

$$E_{\theta\theta} = \frac{1}{2}\left(\lambda_\theta^2 - 1\right) \quad (2a)$$

$$E_{LL} = \frac{1}{2}\left(\lambda_L^2 - 1\right) \quad (2b)$$

A four-parameter Fung model was selected to evaluate the mechanical behavior of the tissue samples, which were assumed to be anisotropic, incompressible, non-linear hyperelastic materials. The Fung strain energy function W, was defined for biaxial loading by the equations below, where c, $c_{\theta\theta}$, $c_{\theta L}$ and c_{LL} represent the model parameters.

$$W(Q) = \frac{1}{2}c\left(e^Q - 1\right) \quad (3a)$$

$$Q(E) = c_{\theta\theta}E_{\theta\theta}^2 + 2c_{\theta L}E_{\theta\theta}E_{LL} + c_{LL}E_{LL}^2 \quad (3b)$$

Theoretical Cauchy stress (T^{model}) was calculated using the Fung model according to the following equations:

$$T_{\theta\theta}^{model} = \lambda_\theta^2 c e^Q \left(c_{\theta\theta}E_{\theta\theta} + c_{\theta L}E_{LL}\right) \quad (4a)$$

$$T_{LL}^{model} = \lambda_L^2 c e^Q (c_{\theta L} E_{\theta\theta} + c_{LL} E_{LL}) \quad (4b)$$

Experimental stress data was mathematically fitted to equations (4a) and (4b) using a non-linear least-squares regression algorithm to determine the Fung model parameters for each sample. All computations were performed using MATLAB version 9.4 (MathWorks, Natick, MA).

Tangent moduli at a stress of 19.1 kPa, representing the estimated peak wall stress of the pathologically-remodeled rat LV at 4 weeks after MI (Ferferieva et al., 2018), were calculated from Fung model stress-strain curves. Finally, the degree of anisotropy between the stiffnesses along each axis was calculated as follows:

$$Anisotropy = min\left[\frac{c_{\theta\theta} + c_{\theta L}}{c_{\theta L} + c_{LL}}, \frac{c_{\theta L} + c_{LL}}{c_{\theta\theta} + c_{\theta L}}\right] \quad (5)$$

2.8. Histology

Following biaxial testing, a subset of samples (n = 5 per group) were embedded in optimum cutting temperature compound and stored at −80°C. The samples were sectioned in 10 μm slices parallel to the epicardial surface, and five slides were selected for each sample at evenly-spaced transmural depths and stained with Masson's trichome stain. Scanned images of the heart sections were imported into ImageJ. Infarct size analysis was performed by color deconvolution using a custom filter to separate the various components of the trichromatic stain. The total number of red and blue pixels, representing muscle and collagen scar, respectively, was determined and the percentage infarct of each tissue section was calculated as blue pixels divided by total red and blue pixels. The overall percentage infarct of a given sample was calculated as the average percentage infarct observed at the five transmural depths, weighted by the total number of pixels contained in each section.

2.9. Statistical analysis

The surgeon and all investigators involved with echocardiography, biaxial testing, and histology remained blinded to the treatment group assignments until data collection was completed. Statistical analyses were performed using Stata version 14.2 (StataCorp LLC., College Station, TX). Continuous variables were reported as mean ± standard error and compared using one-way ANOVA followed by Tukey's multiple comparisons test. A p-value < 0.05 was considered statistically significant. Experimental data will be made available upon reasonable request.

3. Results

3.1. ESA improves Post-MI ventricular remodeling and function

Echocardiography performed 4 weeks after MI revealed significant differences in LV size and function among the three groups, with notable improvements in the ESA group (Table

1). Post-MI ventricular remodeling, characterized by LV wall thinning, chamber dilation, and functional impairment, was clearly observed in the PBS group compared to the sham group (LVWT: sham 1.84 ± 0.05 mm vs PBS 1.42 ± 0.08 mm, $p < 0.001$; LVIDs: sham 3.88 ± 0.14 mm vs PBS 5.63 ± 0.33 mm, $p < 0.001$; EF: sham 74.1 ± 1.5% vs PBS 49.4 ± 4.5%, $p < 0.001$). ESA-treated infarcted hearts, however, were similar in thickness and size to non-infarcted sham controls (LVWT: sham 1.84 ± 0.05 mm vs ESA 1.68 ± 0.05 mm, $p = 0.143$; LVIDs: sham 3.88 ± 0.14 mm vs ESA 4.48 ± 0.30 mm, $p = 0.264$; LVIDd: sham 7.01 ± 0.16 mm vs ESA 6.88 ± 0.29 mm, $p = 0.917$), and were significantly less remodeled than PBS-injected infarcted hearts (LVWT: PBS 1.42 ± 0.08 mm vs ESA 1.68 ± 0.05 mm, $p = 0.008$; LVIDs: PBS 5.63 ± 0.33 mm vs ESA 4.48 ± 0.30 mm, $p = 0.011$; LVIDd: PBS 7.69 ± 0.22 mm vs ESA 6.88 ± 0.29 mm, $p = 0.044$). ESA-treated hearts also exhibited significantly improved cardiac function compared to PBS controls (EF: PBS 49.4 ± 4.5% vs ESA 62.8 ± 3.0%, $p = 0.014$).

3.2. ESA reduces infarct size

Representative images of LV wall samples from the sham, PBS, and ESA groups are shown in Fig. 2A–C. The percentage of transmural LV tissue comprised of collagen, representing post-MI scar tissue, was quantified histologically and observed to be significantly lower among ESA-treated hearts than PBS-injected hearts (29.4 ± 2.9% vs 41.6 ± 3.1%, $p = 0.021$, Fig. 2D). As expected, no collagen scar was detected in the sham control group histologically.

3.3. ESA preserves native myocardial tissue compliance after MI

Cauchy stress-Green strain experimental data plots derived from biaxial testing are shown in Fig. 3. A non-linear response to strain was observed in all three groups, as well as in both the circumferential and longitudinal directions. The average Fung model parameters are presented in Table 2. The circumferential ($c_{\theta\theta}$), longitudinal (c_{LL}), and coupling ($c_{\theta L}$) coefficients of the PBS group were observed to increase when compared to those of the sham group, indicating an increase in multiaxial stiffness. All model parameters of the ESA group were statistically similar to those of the sham group. The degree of anisotropy was also similar among all three groups (sham 0.61 ± 0.05 vs PBS 0.66 ± 0.04 vs ESA 0.60 ± 0.04, $p = 0.638$).

Average stress-strain curves created from the Fung model are shown in Fig. 4, focusing on the estimated range of LV wall stresses encountered by infarcted and non-infarcted rat hearts (Ferferieva et al., 2018; Fomovsky et al., 2011). While PBS-injected hearts exhibited stiffer behavior than ESA-treated hearts in both the circumferential and longitudinal directions, the ESA-treated and sham control hearts behaved similarly throughout the range of strains examined in both principal directions.

The tangent modulus was determined at a stress level of 19.1 kPa, representing the estimated average peak wall stress of an infarcted rat LV at 4 weeks after MI (Ferferieva et al., 2018). Among rats that experienced MI, those that received intramyocardial ESA therapy had significantly more compliant LV tissue after 4 weeks than those that received PBS (Fig. 5). In the circumferential direction, PBS hearts exhibited a modulus of 264.3 ± 12.5 kPa

compared to 211.5 ± 6.9 kPa for ESA hearts ($p = 0.001$). In the longitudinal direction, the modulus for PBS hearts was 258.1 ± 14.4 kPa compared to 194.5 ± 6.5 kPa for ESA hearts ($p < 0.001$). ESA-treated infarcted hearts and sham noninfarcted hearts exhibited similar tissue moduli at this stress level (circumferential: sham 220.2 ± 7.6 kPa vs ESA 211.5 ± 6.9 kPa, $p = 0.786$; longitudinal: sham 209.1 ± 9.6 kPa vs 194.5 ± 6.5 kPa, $p = 0.606$). Indeed, at all physiologically-relevant wall stress values examined (0.1–50.0 kPa), the modulus of ESA-treated infarcted hearts and sham non-infarcted hearts did not differ significantly.

4. Discussion

Our study is the first to utilize biaxial tensile testing to evaluate the mechanical effect of a translatable, angiogenic and myocardial repair-based therapy for ischemic cardiomyopathy. We observed that ESA therapy significantly improves LV remodeling and function, decreases infarct size, and preserves native tissue compliance after MI in both the circumferential and longitudinal directions. These results are consistent with those of our previous studies (Hiesinger et al., 2011; Macarthur et al., 2014; MacArthur et al., 2013; Trubelja et al., 2014), altogether strengthening our biomechanical understanding of how ESA attenuates the complex process of ventricular remodeling following MI.

Biaxial tensile testing represents the gold standard for the evaluation of cardiac biomechanics (Voorhees and Han, 2015). This multiaxial test offers significant advantages compared to uniaxial testing by loading and deforming the tissue along two axes simultaneously and capturing coupled behavior in anisotropic tissues. Our observation that untreated infarcted myocardium is significantly stiffer than healthy non-infarcted myocardium agrees with the results of the few previous studies evaluating biaxial cardiac biomechanics after MI. In both rodents and sheep, myocardial tissue stiffness increases during the initial weeks immediately following MI due to collagen deposition within the developing scar (Fomovsky and Holmes, 2010; Gupta et al., 1994; Sirry et al., 2016; Voorhees et al., 2015). Our histologic analyses confirmed the presence of large transmural infarcts in the untreated MI hearts, in association with pronounced LV wall thinning and dilatation, and impairment of contractile function on echocardiography.

Recent advances in cardiovascular imaging technology have also permitted determination of myocardial stress and strain using cardiac magnetic resonance imaging (MRI) and speckle-tracking echocardiography (Scatteia et al., 2017). These techniques are able to provide useful in vivo metrics of cardiac function and mechanics, but may be limited by issues with temporo-spatial resolution for MRI or quality of acoustic windows and frame rate for echocardiography, especially when applied to small animals. In our study, we employed an established ex vivo method of evaluating myocardial tissue biomechanics in small animals, but utilized previously published in vivo imaging data to guide the physiologic relevance of our experimental design. Specifically, we chose a peak strain of 40% to ensure that our biaxial stretching protocol would encompass the range of strains necessary to generate pathophysiologic wall stresses for assessment of tissue stiffness (Ferferieva et al., 2018; Fomovsky et al., 2011; Weytjens et al., 2008). Our observation that ESA-treated infarcted hearts are significantly less stiff than untreated infarcted hearts, and also retain a similar

stiffness as non-infarcted sham control hearts, altogether suggests that ESA therapy preserves the native compliance of healthy rat myocardium after MI.

Among the co-related factors of infarct size, infarct healing, and ventricular wall stress, which together determine the extent of LV remodeling after MI (Pfeffer and Braunwald, 1990), the primary mediator of the biomechanical effects of ESA is most likely a reduction of infarct size. Indeed, our histologic data demonstrated a significantly higher ratio of muscle to collagen within the stretched LV wall samples in the ESA group compared to the PBS group. This finding corroborates our prior observations in which intramyocardial ESA injection at the time of MI reduced infarct size by 20–33% (Macarthur et al., 2014; MacArthur et al., 2013). Our concept that ESA attenuates ventricular remodeling primarily by reducing infarct size is further supported by previous studies demonstrating that collagen content and infarct size are the chief determinants of post-MI LV mechanics and function, respectively (Fomovsky and Holmes, 2010; Sirry et al., 2016). Akin to the mechanism of intramyocardial SDF therapy, ESA injection into the borderzone is thought to recruit EPCs to the infarct periphery where induced microrevascularization increases local perfusion and cell survival, and decreases muscle replacement by collagen within the infarct and subsequent expansion of the borderzone (Atluri et al., 2006; Hiesinger et al., 2011; Woo et al., 2005). The diminished contribution of infarcted myocardium to the recovering LV wall alters matrix metalloproteinase expression and preserves the extracellular matrix (Macarthur et al., 2014), thus stabilizing wall stresses and inhibiting maladaptive remodeling.

Other therapies have been designed to directly manipulate the mechanics of the struggling ventricle, for example by injection of bio-materials to artificially stiffen the infarct (Morita et al., 2011). Computational models have also suggested that anisotropic infarcts that are selectively stiff in the longitudinal direction or compliant in the circumferential direction may preserve systolic function without compromising diastolic filling (Fomovsky et al., 2011; Voorhees and Han, 2014). Based on this hypothesis, one group demonstrated that infarcted canine hearts reinforced by an anisotropic patch implanted over the ischemic territory did indeed exhibit improved contractility without sacrificing preload (Fomovsky et al., 2012a). In our study, we observed ESA to have equal effectiveness in preserving LV compliance along the circumferential and longitudinal axes, associated with the preservation of native LV geometry but only a partial recovery of systolic function. We injected ESA at four borderzone sites surrounding the periphery of the infarct, but given that collagen fibers of post-injury scar tissue align differently near the cardiac apex than in the basal-mid LV (Fomovsky et al., 2012b), it would be interesting in future experiments to determine whether ESA injection confined to specific regions of the LV would change the mechanical effects of the therapy.

Our study is subject to some limitations common to the biaxial testing of biologic materials. Importantly, the small size of the rat heart may result in a non-homogeneous biaxial stress state during stretching, especially in the areas immediately adjacent to the loading hooks. A previous biaxial study of infarcted rat myocardium used finite element simulations to confirm stress uniformity in the strain-tracked, central area of LV wall samples that were similar in size (10 mm × 10 mm square) and preparation (two loading hooks per side) as those in our study (Fomovsky and Holmes, 2010), adding credence to the accuracy and

interpretability of our results. Nevertheless, some degree of error is inevitable in the absolute values of the stresses and strains measured, although the comparative difference in mechanical behavior observed between the experimental groups is unlikely to be profoundly impacted. Additionally, our understanding of how ESA affects myocardial tissue anisotropy is limited by a lack of data regarding non-equibiaxial mechanical behavior and collagen fiber orientation. Future studies employing different stress ratios along the two axes of deformation and relative to the fiber and cross-fiber directions will be essential for a full evaluation of myocardial tissue anisotropy after angiogenic therapy. Based on analysis of our Fung model parameters derived from equibiaxial testing, however, we observed a moderate degree of anisotropy in both infarcted and non-infarcted hearts—a characteristic that did not change with ESA therapy.

Overall, intramyocardial ESA therapy mitigates post-MI tissue stiffening and preserves LV mechanical properties under planar biaxial tension. The effect of ESA on ventricular geometry, function, and stiffness is likely a consequence of its ability to preserve healthy myocardium and reduce infarct size after acute MI.

Acknowledgements

We thank Hao He, PhD for her assistance with statistical review.

Funding

This study was funded in part by the National Institutes of Health (5R01HL089315–11 to YJW) and by the American Heart Association (18POST33990223 to HW, 17POST33410497 to MJP). The funding sources were not involved in the design, execution, analysis, or writing of the manuscript for this study.

References

Atluri P, Liao GP, Panlilio CM, Hsu VM, Leskowitz MJ, Morine KJ, Cohen JE, Berry MF, Suarez EE, Murphy DA, Lee WMF, Gardner TJ, Sweeney HL, Woo YJ, 2006 Neovasculogenic therapy to augment perfusion and preserve viability in ischemic cardiomyopathy. Ann. Thorac. Surg 81, 1728–1736. 10.1016/j.athoracsur.2005.12.015. [PubMed: 16631663]

Atluri P, Trubelja A, Fairman AS, Hsiao P, MacArthur JW, Cohen JE, Shudo Y, Frederick JR, Woo YJ, 2013 Normalization of postinfarct biomechanics using a novel tissue-engineered angiogenic construct. Circulation 128, S95–S104. 10.1161/CIRCULATIONAHA.112.000368. [PubMed: 24030426]

Azadani AN, Chitsaz S, Matthews PB, Jaussaud N, Leung J, Tsinman T, Ge L, Tseng EE, 2012 Comparison of mechanical properties of human ascending aorta and aortic sinuses. Ann. Thorac. Surg 93, 87–94. 10.1016/j.athoracsur.2011.08.002. [PubMed: 22075218]

Brown L, Fenning A, Chan V, Loch D, Wilson K, Anderson B, Burstow D, 2002 Echocardiographic assessment of cardiac structure and function in rats. Heart Lung Circ 11, 167–173. 10.1046/j.1444-2892.2002.00148.x. [PubMed: 16352093]

Clarke SA, Richardson WJ, Holmes JW, 2016 Modifying the mechanics of healing infarcts: is better the enemy of good? J. Mol. Cell. Cardiol 93, 115–124. 10.1016/j.yjmcc.2015.11.028. [PubMed: 26631496]

Demer LL, Yin FC, 1983 Passive biaxial mechanical properties of isolated canine myocardium. J. Physiol. (Lond.) 339, 615–630. [PubMed: 6887039]

Ferferieva V, D'Elia N, Heyde B, Otahal P, Rademakers F, D'hooge J, 2018 Serial assessment of left ventricular morphology and function in a rodent model of ischemic cardiomyopathy. Int. J. Cardiovasc. Imaging 34, 385–397. 10.1007/s10554-017-1246-4. [PubMed: 28929382]

Fomovsky GM, Clark SA, Parker KM, Ailawadi G, Holmes JW, 2012a Anisotropic reinforcement of acute anteroapical infarcts improves pump function. Circ Heart Fail 5, 515–522. 10.1161/CIRCHEARTFAILURE.111.965731. [PubMed: 22665716]

Fomovsky GM, Holmes JW, 2010 Evolution of scar structure, mechanics, and ventricular function after myocardial infarction in the rat. Am. J. Physiol. Heart Circ. Physiol 298, H221–H228. 10.1152/ajpheart.00495.2009. [PubMed: 19897714]

Fomovsky GM, Macadangdang JR, Ailawadi G, Holmes JW, 2011 Model-based design of mechanical therapies for myocardial infarction. J Cardiovasc Transl Res 4, 82–91. 10.1007/s12265-010-9241-3. [PubMed: 21088945]

Fomovsky GM, Rouillard AD, Holmes JW, 2012b Regional mechanics determine collagen fiber structure in healing myocardial infarcts. J. Mol. Cell. Cardiol 52, 1083–1090. 10.1016/j.yjmcc.2012.02.012. [PubMed: 22418281]

Gupta KB, Ratcliffe MB, Fallert MA, Edmunds LH, Bogen DK, 1994 Changes in passive mechanical stiffness of myocardial tissue with aneurysm formation. Circulation 89, 2315–2326. [PubMed: 8181158]

Harrington KB, Rodriguez F, Cheng A, Langer F, Ashikaga H, Daughters GT, Criscione JC, Ingels NB, Miller DC, 2005 Direct measurement of transmural laminar architecture in the anterolateral wall of the ovine left ventricle: new implications for wall thickening mechanics. Am. J. Physiol. Heart Circ. Physiol 288, H1324–H1330. 10.1152/ajpheart.00813.2004. [PubMed: 15550521]

Hiesinger W, Goldstone AB, Woo YJ, 2012 Re-engineered stromal cell-derived factor-1α and the future of translatable angiogenic polypeptide design. Trends Cardiovasc. Med 22, 139–144. 10.1016/j.tcm.2012.07.010. [PubMed: 22902182]

Hiesinger W, Perez-Aguilar JM, Atluri P, Marotta NA, Frederick JR, Fitzpatrick JR, McCormick RC, Muenzer JR, Yang EC, Levit RD, Yuan L-J, Macarthur JW, Saven JG, Woo YJ, 2011 Computational protein design to reengineer stromal cell-derived factor-1α generates an effective and translatable angiogenic polypeptide analog. Circulation 124, S18–S26. 10.1161/CIRCULATIONAHA.110.009431. [PubMed: 21911811]

Holmes JW, Borg TK, Covell JW, 2005 Structure and mechanics of healing myocardial infarcts. Annu. Rev. Biomed. Eng 7, 223–253. 10.1146/annurev.bioeng.7.060804.100453. [PubMed: 16004571]

Jackson BM, Gorman JH, Moainie SL, Guy TS, Narula N, Narula J, John-Sutton MG, Edmunds LH, Gorman RC, 2002 Extension of borderzone myocardium in postinfarction dilated cardiomyopathy. J. Am. Coll. Cardiol 40, 1160–1167 discussion 1168. [PubMed: 12354444]

Lerman RH, Apstein CS, Kagan HM, Osmers EL, Chichester CO, Vogel WM, Connelly CM, Steffee WP, 1983 Myocardial healing and repair after experimental infarction in the rabbit. Circ. Res 53, 378–388. [PubMed: 6136345]

Macarthur JW, Cohen JE, McGarvey JR, Shudo Y, Patel JB, Trubelja A, Fairman AS, Edwards BB, Hung G, Hiesinger W, Goldstone AB, Atluri P, Wilensky RL, Pilla JJ, Gorman JH, Gorman RC, Woo YJ, 2014 Preclinical evaluation of the engineered stem cell chemokine stromal cell-derived factor 1α analog in a translational ovine myocardial infarction model. Circ. Res 114, 650–659. 10.1161/CIRCRESAHA.114.302884. [PubMed: 24366171]

MacArthur JW, Trubelja A, Shudo Y, Hsiao P, Fairman AS, Yang E, Hiesinger W, Sarver JJ, Atluri P, Woo YJ, 2013 Mathematically engineered stromal cell-derived factor-1α stem cell cytokine analog enhances mechanical properties of infarcted myocardium. J. Thorac. Cardiovasc. Surg 145, 278–284. 10.1016/j.jtcvs.2012.09.080. [PubMed: 23244259]

Mookhoek A, Krishnan K, Chitsaz S, Kuang H, Ge L, Schoof PH, Bogers AJJC, Takkenberg JJM, Tseng EE, 2017 Biomechanics of failed pulmonary autografts compared to native aortic roots. Ann. Thorac. Surg 103, 1482–1488. 10.1016/j.athoracsur.2016.08.061. [PubMed: 27765169]

Morita M, Eckert CE, Matsuzaki K, Noma M, Ryan LP, Burdick JA, Jackson BM, Gorman JH, Sacks MS, Gorman RC, 2011 Modification of infarct material properties limits adverse ventricular remodeling. Ann. Thorac. Surg 92, 617–624. 10.1016/j.athoracsur.2011.04.051. [PubMed: 21801916]

Narula J, Dawson MS, Singh BK, Amanullah A, Acio ER, Chaudhry FA, Arani RB, Iskandrian AE, 2000 Noninvasive characterization of stunned, hibernating, remodeled and nonviable myocardium in ischemic cardiomyopathy. J. Am. Coll. Cardiol 36, 1913–1919. [PubMed: 11092664]

Novak VP, Yin FC, Humphrey JD, 1994 Regional mechanical properties of passive myocardium. J. Biomech 27, 403–412. [PubMed: 8188721]

Omens JH, MacKenna DA, McCulloch AD, 1993 Measurement of strain and analysis of stress in resting rat left ventricular myocardium. J. Biomech 26, 665–676. [PubMed: 8514812]

Pfeffer MA, Braunwald E, 1990 Ventricular remodeling after myocardial infarction. Experimental observations and clinical implications. Circulation 81, 1161–1172. [PubMed: 2138525]

Pfeffer MA, Pfeffer JM, Fishbein MC, Fletcher PJ, Spadaro J, Kloner RA, Braunwald E, 1979 Myocardial infarct size and ventricular function in rats. Circ. Res 44, 503–512. [PubMed: 428047]

Scatteia A, Baritussio A, Bucciarelli-Ducci C, 2017 Strain imaging using cardiac magnetic resonance. Heart Fail. Rev 22, 465–476. 10.1007/s10741-017-9621-8. [PubMed: 28620745]

Sirry MS, Butler JR, Patnaik SS, Brazile B, Bertucci R, Claude A, McLaughlin R, Davies NH, Liao J, Franz T, 2016 Characterisation of the mechanical properties of infarcted myocardium in the rat under biaxial tension and uniaxial compression. J. Mech. Behav. Biomed. Mater 63, 252–264. 10.1016/j.jmbbm.2016.06.029. [PubMed: 27434651]

Trubelja A, MacArthur JW, Sarver JJ, Cohen JE, Hung G, Shudo Y, Fairman AS, Patel J, Edwards BB, Damrauer SM, Hiesinger W, Atluri P, Woo YJ, 2014 Bioengineered stromal cell-derived factor-1α analogue delivered as an angiogenic therapy significantly restores viscoelastic material properties of infarcted cardiac muscle. J. Biomech. Eng 136 10.1115/1.4027731.

Voorhees AP, DeLeon-Pennell KY, Ma Y, Halade GV, Yabluchanskiy A, Iyer RP, Flynn E, Cates CA, Lindsey ML, Han H-C, 2015 Building a better infarct: modulation of collagen cross-linking to increase infarct stiffness and reduce left ventricular dilation post-myocardial infarction. J. Mol. Cell. Cardiol 85, 229–239. 10.1016/j.yjmcc.2015.06.006. [PubMed: 26080361]

Voorhees AP, Han H-C, 2014 A model to determine the effect of collagen fiber alignment on heart function post myocardial infarction. Theor. Biol. Med. Model 11, 6 10.1186/1742-4682-11-6. [PubMed: 24456675]

Voorhees AP, Han H-C, 2015 Biomechanics of cardiac function. Comp. Physiol 5, 1623–1644. 10.1002/cphy.c140070.

Weytjens C, Franken PR, D'hooge J, Droogmans S, Cosyns B, Lahoutte T, Van Camp G, 2008 Doppler myocardial imaging in the diagnosis of early systolic left ventricular dysfunction in diabetic rats. Eur. J. Echocardiogr 9, 326–333. 10.1093/ejechocard/jen123.

Woo YJ, Grand TJ, Berry MF, Atluri P, Moise MA, Hsu VM, Cohen J, Fisher O, Burdick J, Taylor M, Zentko S, Liao G, Smith M, Kolakowski S, Jayasankar V, Gardner TJ, Sweeney HL, 2005 Stromal cell-derived factor and granulocytemonocyte colony-stimulating factor form a combined neovasculogenic therapy for ischemic cardiomyopathy. J. Thorac. Cardiovasc. Surg 130, 321–329. 10.1016/j.jtcvs.2004.11.041. [PubMed: 16077394]

Ziff OJ, Bromage DI, Yellon DM, Davidson SM, 2018 Therapeutic strategies utilizing SDF-1α in ischaemic cardiomyopathy. Cardiovasc. Res 114, 358–367. 10.1093/cvr/cvx203. [PubMed: 29040423]

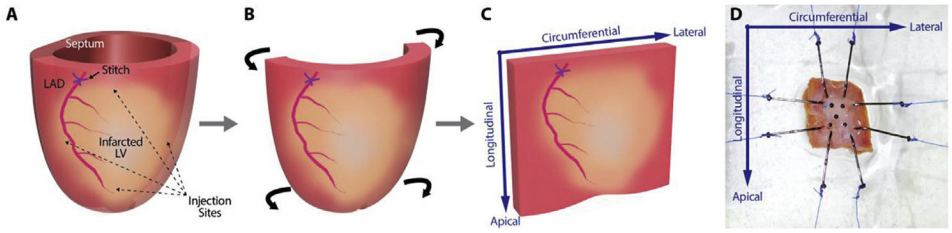

Fig. 1.

Preparation of left ventricular wall samples for biaxial testing. (A) The left ventricle (LV) of the rat heart is shown, with the position of the left anterior descending (LAD) coronary artery, the ligating suture, the ischemic territory, and the four borderzone injection sites labeled. (B–C) The septum and lateral-most aspect of the LV wall are excised, and the remaining anterolateral LV wall is flattened into a square block of tissue. (D) The LV wall sample is mounted onto the biaxial testing device, aligned along the circumferential and longitudinal axes of the heart.

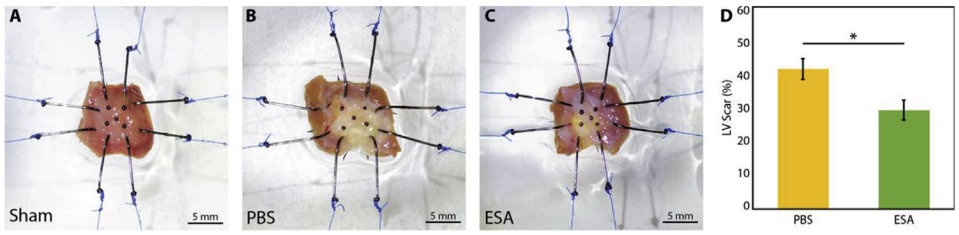

Fig. 2. Infarct size assessment.

(A–C) Representative images of left ventricular (LV) wall samples from sham non-infarcted hearts, saline-injected infarcted hearts (PBS), and therapy-treated infarcted hearts (ESA), mounted onto the biaxial testing device. Hearts in the PBS group qualitatively appear to have larger infarcts than hearts in the ESA group. (D) LV scar percentage determined histologically for each group using Masson's trichrome staining. * indicates p-value < 0.05. Hearts in the ESA group have significantly reduced infarct size compared to hearts in the PBS group.

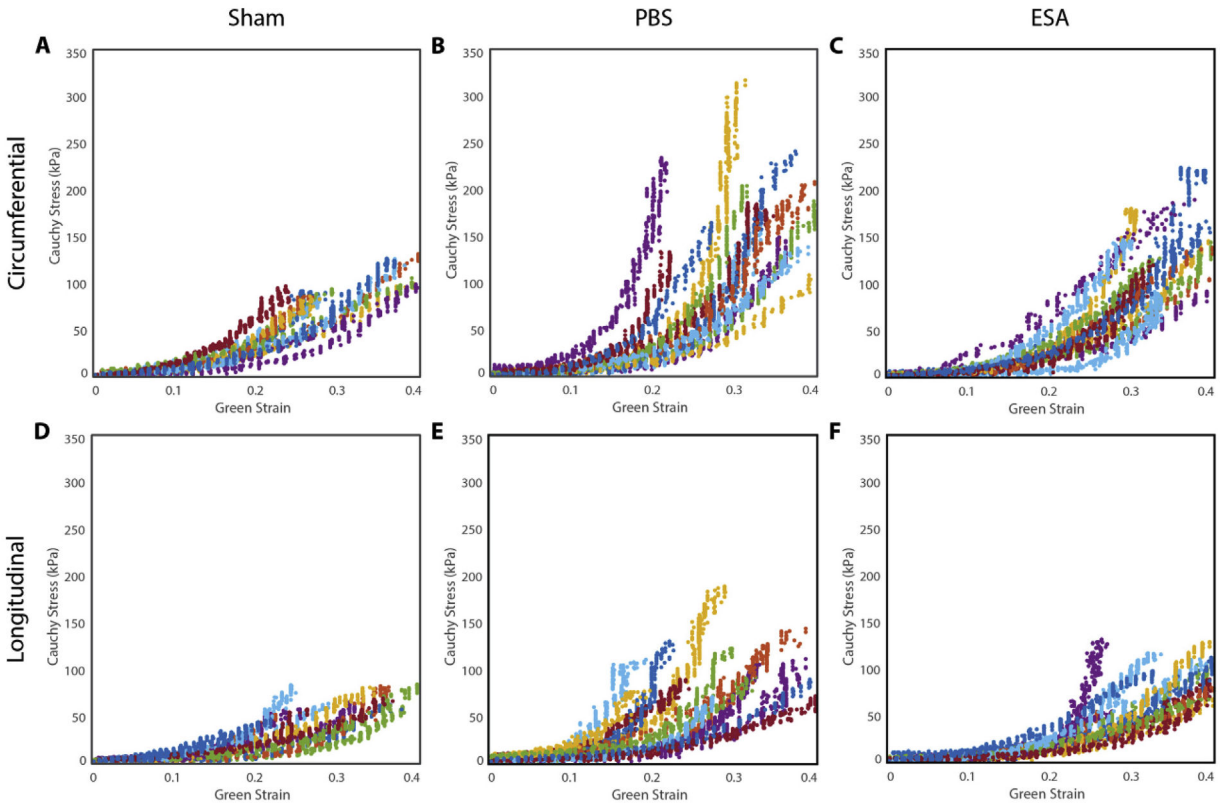

Fig. 3. Cauchy stress-Green strain experimental data plots.

Experimental stress-strain data are presented for the circumferential (A–C) and longitudinal (D–F) directions for sham non-infarcted hearts, saline-injected infarcted hearts (PBS), and therapy-treated infarcted hearts (ESA), obtained from planar biaxial tensile testing. All samples in each group demonstrated a non-linear response to strain in both principal directions.

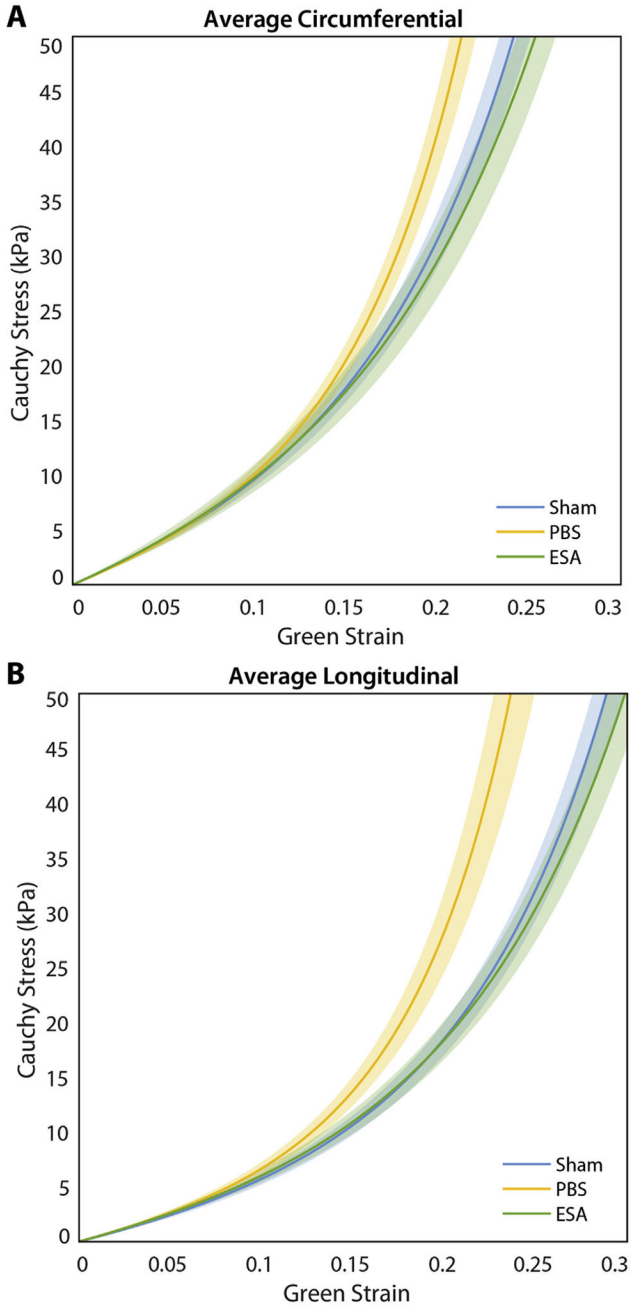

Fig. 4. Composite stress-strain curves.

Stress-strain curves are illustrated for the circumferential (A) and longitudinal (B) directions, derived from the average Fung model curves for sham non-infarcted hearts, saline-injected infarcted hearts (PBS), and therapy-treated infarcted hearts (ESA). Shaded region represents standard error. Hearts in the PBS group exhibit stiffer behavior compared to hearts in the ESA and sham groups in both the circumferential and longitudinal directions.

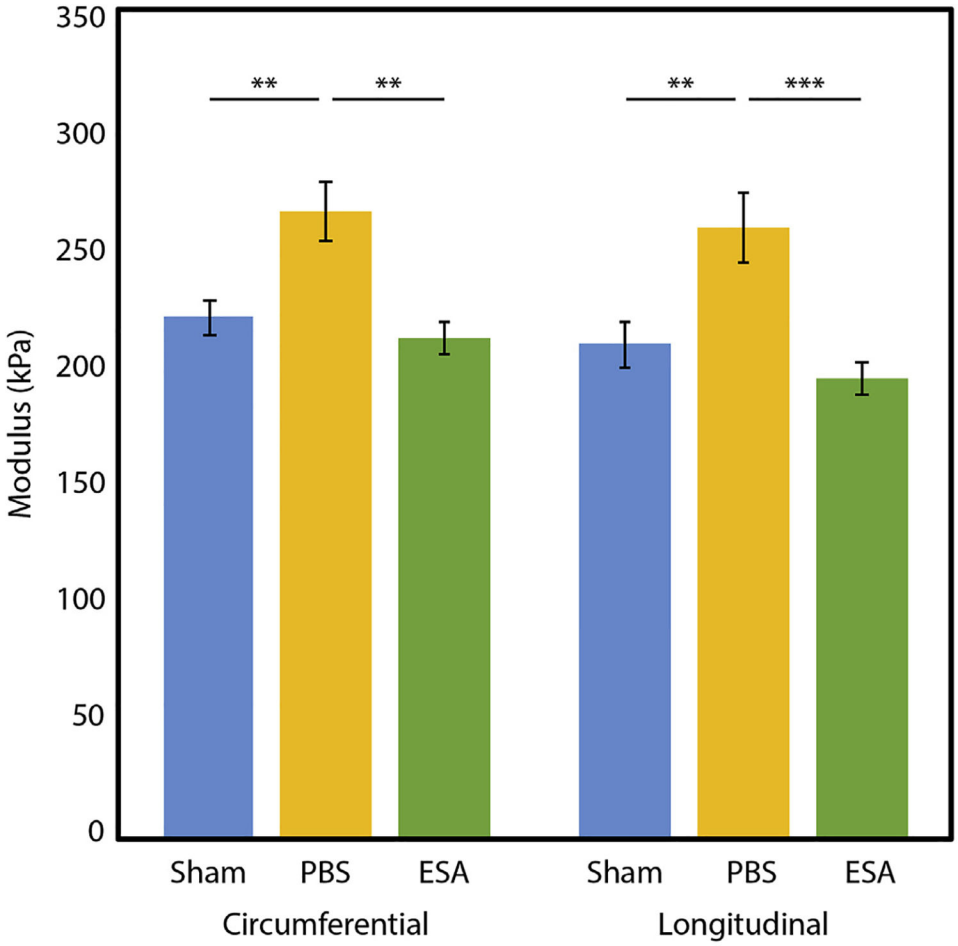

Fig. 5. Tangent modulus at physiologic stress.

The tangent modulus of sham non-infarcted hearts, saline-injected infarcted hearts (PBS), and therapy-treated infarcted hearts (ESA) is calculated at 19.1 kPa, the estimated pathophysiologic wall stress of a rat left ventricle (LV) 4 weeks after myocardial infarction. ** indicates p-value < 0.01. *** indicates p-value < 0.001. Hearts in the ESA group were significantly less stiff than hearts in the PBS group, and had similar modulus as hearts in the sham group.

Table 1

Echocardiography data.

Echocardiography data are presented for sham non-infarcted hearts, saline-injected infarcted hearts (PBS), and therapy-treated infarcted hearts (ESA), including left ventricular wall thickness in diastole (LVWT), left ventricular internal dimension in systole (LVIDs) and diastole (LVIDd), and ejection fraction (EF). Statistically significant differences ($p < 0.05$) in post-hoc analysis are indicated by † for sham vs PBS, ‡ for sham vs ESA, and § for PBS vs ESA.

Echocardiography	Sham	PBS	ESA	P-value	Pairwise
LVWT (mm)	1.84 ± 0.05	1.42 ± 0.08	1.68 ± 0.05	<0.001	†§
LVIDs (mm)	3.88 ± 0.14	5.63 ± 0.33	4.48 ± 0.30	<0.001	†§
LVIDd (mm)	7.01 ± 0.16	7.69 ± 0.22	6.88 ± 0.29	0.038	§
EF (%)	74.1 ± 1.5	49.4 ± 4.5	62.8 ± 3.0	<0.001	†‡§

Table 2

Average Fung model parameters.

The average Fung model parameters are presented for sham non-infarcted hearts, saline-injected infarcted hearts (PBS), and therapy-treated infarcted hearts (ESA). Statistically significant differences ($p < 0.05$) in post-hoc analysis are indicated by † for sham vs PBS and § for PBS vs ESA. N.S. indicates not statistically significant.

Fung Model Parameters	Sham	PBS	ESA	P-value	Pairwise
c	13.62 ± 2.71	8.62 ± 1.63	15.82 ± 3.00	0.130	N.S.
$c_{\theta\theta}$	3.99 ± 0.50	5.87 ± 0.62	3.46 ± 0.31	0.003	†§
$c_{\theta L}$	3.05 ± 0.42	4.92 ± 0.69	2.07 ± 0.27	< 0.001	†§
c_{LL}	1.09 ± 0.20	2.58 ± 0.60	1.60 ± 0.25	0.034	†
Anisotropy	0.61 ± 0.05	0.66 ± 0.04	0.60 ± 0.04	0.638	N.S.